

BIOCHEMISTRY

Direct visualization of the *E. coli* Sec translocase engaging precursor proteins in lipid bilayers

Raghavendar Reddy Sanganna Gari^{1*}, Kanokporn Chattrakun¹, Brendan P. Marsh^{1†}, Chunfeng Mao², Nagaraju Chada^{1‡}, Linda L. Randall², Gavin M. King^{1,2§}

Escherichia coli exports proteins via a translocase comprising SecA and the translocon, SecYEG. Structural changes of active translocases underlie general secretory system function, yet directly visualizing dynamics has been challenging. We imaged active translocases in lipid bilayers as a function of precursor protein species, nucleotide species, and stage of translocation using atomic force microscopy (AFM). Starting from nearly identical initial states, SecA more readily dissociated from SecYEG when engaged with the precursor of outer membrane protein A as compared to the precursor of galactose-binding protein. For the SecA that remained bound to the translocon, the quaternary structure varied with nucleotide, populating SecA₂ primarily with adenosine diphosphate (ADP) and adenosine triphosphate, and the SecA monomer with the transition state analog ADP-AIF₃. Conformations of translocases exhibited precursor-dependent differences on the AFM imaging time scale. The data, acquired under near-native conditions, suggest that the translocation process varies with precursor species.

INTRODUCTION

The transport of specific polypeptide chains across membranes is a fundamental cellular activity. Yet, determining the mechanisms underlying protein translocation remains a major unsolved problem. The general secretory (Sec) system of *Escherichia coli* moves protein into and across membranes and has homologs across all life forms (1). The Sec system uses a translocase that consists of SecA, an adenosine triphosphatase (ATPase), bound to the protein conducting channel, SecYEG, at the cytoplasmic membrane.

SecA is an essential ATPase; during protein export, it makes contact with SecYEG, precursor proteins, lipids, and chaperone SecB and converts chemical energy into mechanical work on the precursor. Adenosine triphosphate (ATP) binding and subsequent hydrolysis are thought to generate conformational changes in the translocase that are coupled to forward movement of the polypeptide chain undergoing translocation (1, 2). Though its processive nature has been debated, SecA is generally thought to dissociate from SecYEG after ATP hydrolysis and rejoin the cytoplasm where it can participate in additional translocation cycles (3–6). This dynamic process continues until the complete polypeptide chain passes through the channel.

Structures of SecA and of SecA in complex with the translocon SecYEG have been achieved from different species at high resolution (1, 2). Three conformations of SecA are prominent: wide open (7), open (8), and closed (9). A large-scale difference in the position of the protein binding domain is the distinguishing aspect between these three conformations. Two models have emerged to describe the translocation step. In a “push and slide” model, SecA delivers ATP

hydrolysis-driven power strokes to the precursor (2, 5, 10). In an alternative model, SecA acts as an allosteric regulator of the protein conducting channel, enabling Brownian ratchet motion of the precursor chain through SecYEG (2, 11, 12). Aspects of the translocation reaction have been observed to vary with the precursor species undergoing transport (6, 13, 14). However, precursor-dependent translocation processes have been largely overlooked in the literature (15).

The oligomeric state of SecA has been a matter of contention. The concentration of SecA in the cytosol of *E. coli* is ~5 to 10 μM. This suggests a high likelihood of dimers, based on the dissociation constant of ≤1 μM (1, 16–19); however, the presence of binding partners can directly affect the oligomeric state (18, 20, 21). Crystal structures of SecA from different species show two prominent orientations of dimer organization (parallel or antiparallel), though others have been identified (7, 22–27). It has been argued that the two protomers within the SecA dimer (SecA₂) can undergo relative motion without dissociating, enabled by hydrophobic and/or electrostatic interactions along the dimer interface that allow SecA protomers to slide and to rotate (4). No structures exist for SecA₂ when in complex with the translocon (2).

Notwithstanding important insights garnered, structural data often consist of static snapshots acquired in the absence of lipid bilayers. However, it has long been known that the structure of SecA is highly dynamic and that activity is altered upon binding anionic lipids, SecYEG, and precursors. This implies that important conformational changes are likely to result from SecA-lipid, SecA-SecYEG, and SecA-SecYEG-precursor interactions (2, 28–30). However, a structure-dynamic study of the Sec translocase in the presence of lipids, precursors, and nucleotides is lacking.

Atomic force microscopy (AFM) has emerged as an increasingly valuable tool in biology. The method is well suited for imaging membrane proteins under near-native conditions and can achieve molecular-scale (~10 Å) lateral resolution coupled with ~1-Å vertical resolution (i.e., normal to the bilayer surface) (31, 32). In previous work, our group applied AFM to visualize individual components of the general Sec system (33, 34), as well as the idle Sec translocase

Copyright © 2019
The Authors, some
rights reserved;
exclusive licensee
American Association
for the Advancement
of Science. No claim to
original U.S. Government
Works. Distributed
under a Creative
Commons Attribution
NonCommercial
License 4.0 (CC BY-NC).

¹Department of Physics and Astronomy, University of Missouri, Columbia, MO 65211, USA. ²Department of Biochemistry, University of Missouri, Columbia, MO 65211, USA.

*Present address: Department of Anesthesiology, Weill Cornell Medicine, New York, NY 10065, USA.

†Present address: Department of Applied Physics, Stanford University, Stanford, CA 94305, USA.

‡Present address: Department of Biology, Johns Hopkins University, 3400 N. Charles Street, Baltimore, MD 21218, USA.

§Corresponding author. Email: kinggm@missouri.edu

complex reconstituted into lipid bilayers in the absence of precursors (13, 35).

Here, we shed light on active translocase complexes. Using a combination of biochemical experiments and AFM imaging, we studied the dynamic topography of the Sec translocase engaging two distinct precursors: one destined for the outer membrane [outer membrane protein A (pOmpA, alternatively known as proOmpA)] and the other destined for the periplasm [galactose-binding protein (pGBP)]. Our conclusions are threefold: (i) SecA readily dissociates from the translocase when engaged with pOmpA, but the vast majority of SecA remains associated with the translocase when engaged with pGBP. (ii) The quaternary structure of SecA in the active translocase is dimeric (or higher order) in the hydrolysis (ATP) and resting [adenosine diphosphate (ADP)] state and becomes monomeric in the transition state (ADP-AlF₃). These changes in SecA quaternary structure were independent of the two precursor species. (iii) Active translocases exhibit conformations on the time scale of AFM imaging that vary with precursor species. We attribute the conformational differences to SecA-driven structural rearrangements within the translocase. Overall, the data suggest that the Sec translocation process works differently for different precursors.

RESULTS

Translocase activity in solution

We first carried out *in vitro* assays to confirm that the reconstituted proteoliposome preparations were compatible for translocation. The starting material for all assays consisted of SecYEG and SecA coassembled into liposomes. These robust proteoliposomes (SecYEG-SecA) showed a level of activity similar to that of inner membrane vesicles (13, 14). To probe the translocase in the process of translocation, we used precursors containing disulfide-stabilized loops of either 44 or 59 aminoacyl residues near the C termini of pGBP and pOmpA,

respectively, unless otherwise stated (13, 36). Translocation of oxidized precursors is initiated, but stalls at the loop, which is too large to pass through the channel in the translocon. Figure 1A shows time courses of translocation for each precursor species. The time to reach within 98% of the plateau value was longer for pGBP (4.5 min) than it was for pOmpA (3 min). Additional assays (fig. S1) demonstrate that precursors of intermediate lengths were protected from proteinase K digestion because of the looped precursor topology. We note that we have previously characterized the activity of linear pOmpA and pGBP using coassembled SecYEG-SecA proteoliposomes (13).

Translocase activity on mica surface

For AFM imaging, proteoliposomes were adsorbed onto mica surfaces. In principle, the translocase activity of surface-adsorbed translocase complexes in supported lipid bilayers can be verified by monitoring ATP-dependent protection of precursor proteins, as in *in vitro* assays (13). Therefore, we assessed the activity of translocase complexes in lipid bilayers on mica substrates. Proteoliposome SecYEG-SecA samples were incubated on freshly cleaved mica surfaces in a manner identical to that used for AFM imaging. We then added a mixture consisting of SecA, SecB, ATP, and a radiolabeled precursor, which was incubated for a time period commensurate with AFM imaging (2 hours) followed by proteinase K digestion and rinsing (see Materials and Methods for details). A nonoxidized precursor was used to allow for the possibility of multiple turnovers per SecYEG. Mica disks subjected to the surface translocation assay in the presence or absence of ATP were quantified using a PhosphorImager (Fig. 1B). After calibration (fig. S2), the amount of radioactivity of the protease-treated membranes was converted to the amount of precursor protected. The results (Fig. 1C and fig. S3) show the hallmark of active translocation: ATP-dependent protection from proteinase K digestion.

Can surface-supported translocases catalyze multiple turnovers? After accounting for background (i.e., mol precursor detected in

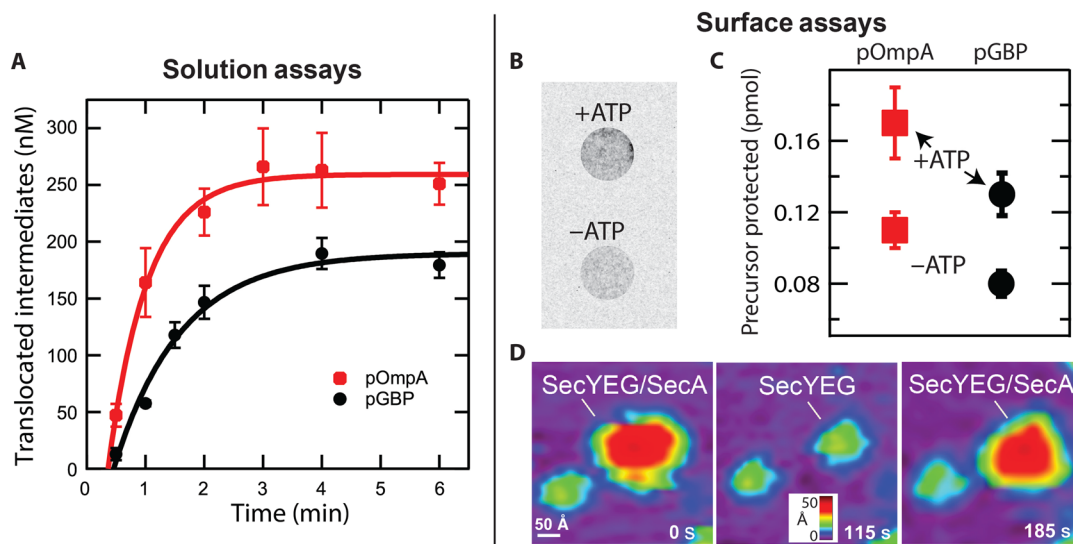


Fig. 1. Translocase activity evaluated in solution and on mica. (A) Translocation activity of radiolabeled, oxidized pOmpA (red squares, $n = 3$) or oxidized pGBP (black circles, $n = 3$) assayed *in vitro* by protection from proteinase K. Error bars are SDs, and lines are fits to an exponential rise to maximum. (B) Image of radioactivity from mica disks with pOmpA \pm ATP. (C) Data (mean \pm SEM) showing mol precursor pOmpA or pGBP protected on mica in the presence or absence of ATP. (D) Visualization of translocase dynamics in the absence of precursor. SecA dissociates from the membrane to reveal SecYEG beneath, and then SecA is seen to associate. Note that SecYEG in the bottom left remains unoccupied for all images. The time of each frame is listed (bottom right, units: seconds); the lateral scale bar is 50 Å, and the vertical false color scale is 50 Å.

the system without ATP), we found that an average of 0.06 pmol of pOmpA is actively translocated through the surface-supported bilayer after 120 min. Although this quantity is small, the number of translocase units available on the surface was only 0.03 pmol, estimated from the areal density of translocases observed in AFM images and the area of the mica disk. Therefore, we found the turnover number of pOmpA to be approximately 2.0. The corresponding turnover number of pGBP was 1.7. We note that there is some space available for the precursor proteins to move into. Experiments have shown that supported lipid bilayers typically contain a ~ 10 -Å-thick aqueous layer between the lower bilayer leaflet and the underlying supporting surface (37). We also note that erroneous deductions of activity could result if the addition of ATP altered the number or size of membrane defects; however, this was challenging to quantify in our assays because of the low overall number of defects and technical difficulties in identifying the same defect in subsequent AFM images.

Additional evidence of surface-supported translocase competency comes directly from AFM image data. SecYEG and SecA within the translocase complex exist in a dynamic equilibrium. A sequence of images of the SecYEG-SecA starting material in the absence of precursor (Fig. 1D) shows a translocase undergoing SecA dissociation (at 115 s), followed by SecA association (at 185 s). An additional copy of the translocase SecYEG is visible in the lower left of the images, serving as a reference. The assignment of specific protrusions to SecYEG and SecA has been reported previously and is discussed below (13, 34). This visualization implies that the cytoplasmic loops of SecYEG remain competent for binding SecA during AFM imaging on mica, which is consistent with our previous studies on glass (35). Together, the data indicate that AFM imaging and the proximity of a mica surface do not preclude general Sec system activity.

Translocase topography as a function of translocation stage and precursor species

To define an initial state of the system, we allowed translocation of either pOmpA or pGBP to proceed for only 30 s, at which point ADP-ALF₃ (ADPALF) was added to halt further hydrolysis. The nonhydrolyzable ATP analog ADPALF is thought to trap SecA in the transition state (38). Immediately after ADPALF addition, we deposited the reaction mix onto freshly cleaved mica. Samples were incubated, rinsed, and then imaged. All data were collected in imaging buffer using tapping mode at $\sim 32^\circ\text{C}$ (see Materials and Methods for details).

Representative AFM images of the Sec translocase engaging precursors at different stages of translocation are displayed (Fig. 2 and figs. S4 and S5). The presence of lipid bilayers was confirmed by the observation of occasional defects (voids) that were ~ 40 Å deep from the surface of the upper leaflet of the bilayer (39); one such void is indicated (Fig. 2A, i, arrow). The images contained many punctate protrusions corresponding to translocases and translocons above the *E. coli* lipid bilayer. Images of proteoliposomes containing only SecYEG and of lipids alone are also presented (fig. S6). Representative individual protrusions are shown as insets at the right corner of each image in Fig. 2A. To facilitate statistical analyses, salient topographic parameters were extracted and pooled together to construct kernel density estimates (smoothed histograms). On the basis of our previous work imaging SecYEG in lipid bilayers and SecYEG in complex with SecA in lipid bilayers (34, 35), many of the protrusions exhibited topography commensurate with the translocase [i.e., an approximate height range between 32 and 80 Å with a major population at about 37 Å (13)]. In the absence of SecYEG, SecA does

not appear to bind the lipid bilayer in a preferred conformation (13). Protrusions corresponding to the periplasmic side of SecYEG, which extend <10 Å above the membrane and do not engage SecA, were not included in the analysis (34). In addition, features exhibiting large heights (>100 Å), which were likely to be aggregates, were rare ($<15\%$ of total) and not included in analysis. To evaluate protein crowding, a potential artifact, proteoliposomes with a fourfold lower protein-to-lipid ratio were prepared. Despite moderate variations expected from different sample preparations, the data suggest (fig. S7) that crowding effects are negligible at the protein-to-lipid ratio used throughout this work (P:L = 1:1000).

Height analysis of translocases at the initial stage of translocation

At the initial stage of translocation (30 s), we did not observe substantial differences in the height distribution between Sec translocases engaging pOmpA and pGBP (Fig. 2B, compare red and black curves). This similarity is plotted in Fig. 2F, which shows nearly identical mean translocase height for both precursors at the initial stage. At 30 s, the data indicate that translocation has initiated but not progressed very far (Fig. 1A); incubation is started by moving the assay from ice to 30°C , and it takes ~ 15 s for the temperature to equilibrate. The distributions at 30 s for both precursors were maximally populated at the same height ~ 37 Å above the lipid bilayer. This ~ 37 -Å population overlaps with the protrusion heights in proteoliposomes SecYEG-SecA in the absence of precursor (Fig. 2B, green dashed curve). For translocases engaging precursors, the presence of a broad subpopulation with heights between 40 and 70 Å was common to both pGBP and pOmpA. This common topographic subpopulation could result from different translocase conformations that are equally populated among translocases engaging the two precursor species at this early stage of translocation.

Height analysis of translocases at the plateau stage of translocation

We then investigated translocase topography at the plateau stage of translocation activity. Times were selected on the basis of the results of activity assays (Fig. 1A). In particular, translocation proceeded for 3 min with pOmpA or 4.5 min for pGBP, at which point ADPALF was added to halt further hydrolysis. AFM images revealed substantial differences in measured height distributions between Sec translocases with pOmpA and pGBP at the plateau stage of translocation (Fig. 2C). With pOmpA (black curve), heights were shifted lower from the initial state, with a substantial population (44% of total) in the SecYEG height range [between ~ 12 and 32 Å; see Fig. 2B, magenta dotted curve; (34)]. This implies that SecA has completely dissociated from many translocons after 3 min of pOmpA translocation. We note that samples were rinsed with imaging buffer after incubation on mica; hence, dissociated SecA may not be available for rebinding to SecYEG. Nonetheless, there remained a significant population ($>50\%$) of intact translocase complexes. In contrast, the height distribution for pGBP evaluated at the plateau stage of activity (Fig. 2C, red) was shifted significantly higher than the heights observed at the initial stage (Fig. 2B, red). Bar graphs of mean height (Fig. 2F) demonstrate the notable >10 -Å difference in translocase topography between precursors when evaluated at plateau activity. For pGBP at plateau, the peak of the height distribution was ~ 46 Å. At the initial stage, the height distribution with pGBP exhibited a shoulder at this same height; however, at plateau, this population was dominant. Different translocase conformations caused by pGBP binding may underlie the observed increase in peak height by ~ 9 Å in comparison to heights at

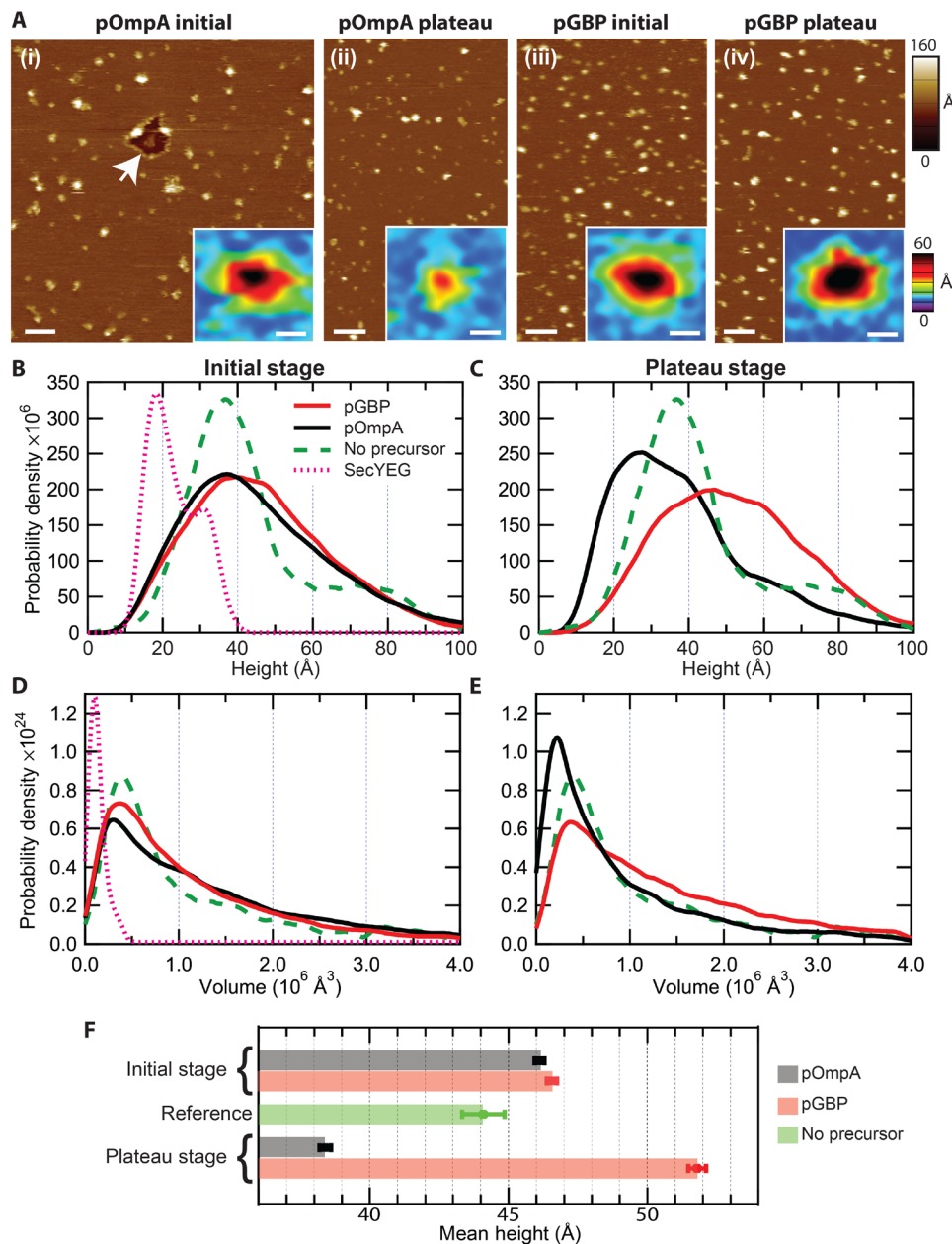


Fig. 2. Sec translocase topography varies as a function of precursor species and translocation stage. (A) AFM images of Sec translocases: (i) with pOmpA at the initial stage (30 s) of translocation, the arrow identifies a void in an otherwise continuous lipid bilayer; (ii) with pOmpA at the plateau stage of activity (3 min); (iii) with pGBP at 30 s; and (iv) with pGBP at plateau (4.5 min). Lateral scale bars are 1000 Å and the false color vertical scale spans 160 Å. Individual features are shown as insets with scale bars: 100 Å (lateral) and 60 Å (vertical). (B) Height and (D) volume distributions of active Sec translocases at 30 s with either pOmpA (red curve, number of features included, $n = 12,387$) or pGBP (black curve, $n = 10,063$). Data for translocases SecYEG-SecA with no precursor (green dashed curve, $n = 587$) as well as SecYEG alone (magenta dotted curve, $n = 1875$) are shown for reference. After reaching the plateau stage of translocation activity, the (C) height and (E) volume distributions of translocases engaged with pOmpA (red curve, $n = 9565$) or with pGBP (black curve, $n = 6592$) are shown. In all cases, translocation was halted by adding ADPAIF at the prescribed times. Note that the vertical scales for SecYEG alone data were compressed two- or fivefold in the height or volume plots, respectively. (F) Arithmetic means of the height distributions. Error bars show SEM.

the initial stage; however, volume analysis (discussed below) is required to rule out the possibility of SecA quaternary structure changes. We note that both precursor species (monomer molecular mass, ≤ 38 kDa) and the cytoplasmic loops of SecYEG are significantly smaller than SecA (monomer molecular mass, 102 kDa). In addition, SecYEG loops are completely covered (or buried) under SecA. Hence,

AFM-measured translocase topography on the cytoplasmic side of the membrane is conferred by SecA, and conformational changes caused by precursors can be recorded via changes in translocase height. Integration of height histograms with pGBP revealed that only 16% of protrusions corresponded to the height of SecYEG lacking SecA, in comparison to 44% with pOmpA. Population percentages were

verified to within <1% by bootstrapping. Therefore, the association of SecA with the translocon SecYEG varied significantly (>2-fold) between the two precursor species at the plateau stage of activity, and the relative absence of SecA gives rise to the low mean height value for pOmpA (Fig. 2F).

Volume analysis of translocases at the initial and plateau stages of translocation

In addition to heights above the lipid bilayer, we also analyzed the volumes of translocase complexes as a function of translocation stage and precursor species. As in the height analysis, volume distributions in the initial phase of translocation (30 s) were similar for translocases engaging both pOmpA and pGBP (Fig. 2D, black and red curves, respectively) as well as for the starting material (SecA·SecYEG; Fig. 2D, green dashed curve). Translocases engaging both precursor species exhibited a prominent volume population near $0.4 \times 10^6 \text{ \AA}^3$ representing monomeric SecA. Oligomeric state assignments are discussed below and in figs. S8 to S11.

Comparison of volumes at the initial stage of translocation (Fig. 2D) to times corresponding to the plateau of activity (Fig. 2E) revealed significant population shifts. In particular, at the later time, the prominent volume peak for pOmpA shifted lower to approximately $0.2 \times 10^6 \text{ \AA}^3$; this low volume implies that SecA has dissociated from the membrane, exposing the underlying translocon, whose volume we have previously characterized (34). Concurrently, the population of dimeric SecA (figs. S8, S9, and S11) was reduced as evidenced by fewer protrusions exhibiting volumes between 1×10^6 and $2 \times 10^6 \text{ \AA}^3$. In contrast, in the case of pGBP, no major changes in the volume distribution were observed when comparing the 30-s time point to the plateau stage. The major volume peak at both stages, $\sim 0.4 \times 10^6 \text{ \AA}^3$, corresponds to a SecA monomer. The shoulder at around $\sim 1 \times 10^6$ to

$2 \times 10^6 \text{ \AA}^3$ corresponding to a SecA dimer is also present at plateau. Because the volume of translocases engaging pGBP did not change significantly with time, this implies that the increase in height observed for pGBP at plateau is associated with a change in translocase conformation rather than a change in oligomeric state.

Overall, when imaging translocase complexes at different stages of translocation stabilized by the nonhydrolyzable analog ADPAIF, height and volume distributions indicated that SecA is more likely to dissociate from translocases engaging pOmpA than from those engaging pGBP. Further, for the SecA that remained bound to the translocon, translocase conformations when engaging pGBP were distinct from conformations with pOmpA.

Dynamic topography of translocase in the presence of ATP

We further asked: How does ATP hydrolysis affect the topography of the Sec translocase? To answer this question, we performed a similar in vitro translocation assay using oxidized precursor species with looped topology. However, in this case, we did not add ADPAIF. Samples were immediately deposited onto mica after translocation activity reached plateau. AFM image data are shown (fig. S12). For pOmpA (Fig. 3A, red curve), we again observed a substantial population of protrusions with heights in the region corresponding to the cytoplasmic side of the translocon SecYEG alone, indicating dissociation of SecA (Fig. 3A, gray shaded region, ~ 12 to $\sim 32 \text{ \AA}$ above the bilayer) (34). Thirty-six percent of all pOmpA protrusions when imaged in ATP were found to be in this height range. This is similar to pOmpA translocases exposed to ATP followed by ADPAIF (Fig. 3A, blue dotted curve, data carried over from Fig. 2). We also observed a shoulder-like population of translocases in ATP from about 40 to 70 \AA . This may be attributed to different translocase conformations.

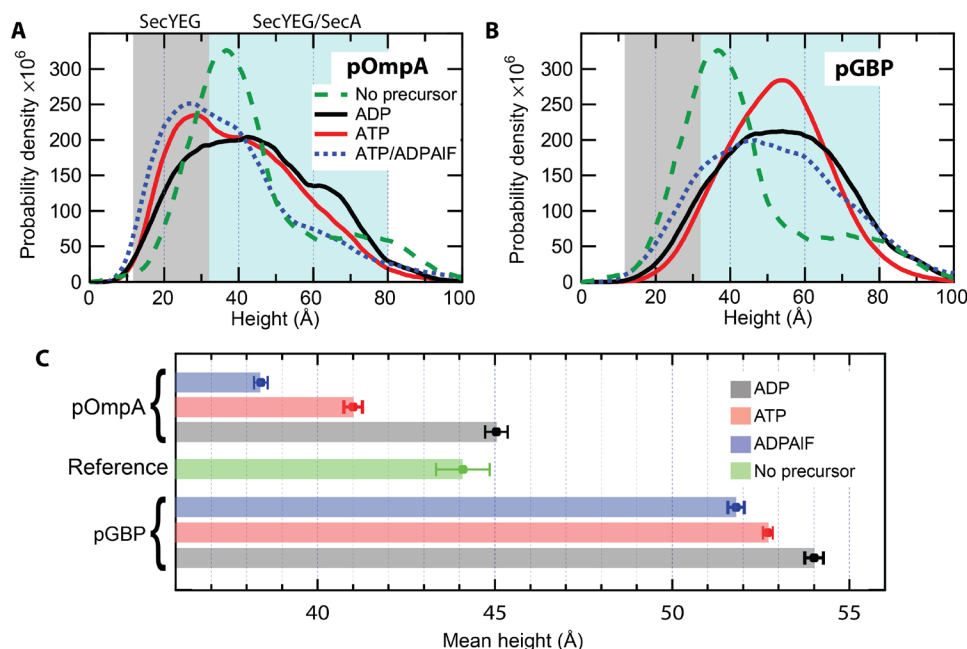


Fig. 3. SecA readily unbinds from SecYEG in the presence of pOmpA but not with pGBP. (A) Height distribution of Sec translocase engaging pOmpA and different nucleotides: ADP only (black curve, $n = 2975$), ATP only (red curve, $n = 4010$), or ATP followed by ADPAIF (blue dotted curve, $n = 9565$). (B) Height distribution of Sec translocase engaging pGBP and different nucleotides: ADP only (black curve, $n = 3962$), ATP only (red curve, $n = 9277$), or ATP followed by ADPAIF (blue dotted curve, $n = 6592$). Data with no precursor are overlaid for reference (green dashed curve, $n = 587$). Gray and blue regions in (A) and (B) indicate the approximate height range of the translocon SecYEG alone and the translocase complex, respectively. (C) Bar graphs show the arithmetic mean of the height distributions. Error bars are SEM.

We note that this population is above the prominent peak population at 37 Å but still in the height range of SecA bound to SecYEG (Fig. 3A, blue shaded region, ~32 to 80 Å) (13).

In contrast to pOmpA, the distribution of Sec translocases with pGBP did not shift toward lower heights when exposed to ATP (Fig. 3B, red curve). Only 7% of total protrusions in the pGBP data were found in the SecYEG-only height range, which is approximately fivefold lower compared to pOmpA. Before precursors were added (i.e., in the SecYEG-SecA sample), approximately 27% of total protrusions were found in the SecYEG height range (Fig. 3, green dashed curve); the remainder exhibited heights corresponding to the translocase.

Sec translocases engaging pGBP with ATP exhibited a peak in the height distribution at ~53 Å, characteristic of SecA bound to SecYEG (Fig. 3B, red curve) (13). This ATP peak was higher by ~7 Å compared to heights measured with ATP followed by ADPAIF for the same precursor (Fig. 3B, blue dotted curve, data carried over from Fig. 2). In addition, the height difference between the main height peak of Sec translocases engaging pGBP and that of the starting material (SecYEG-SecA in the absence of precursor) was large (~16 Å).

Resting state translocase with ADP

To probe the resting state of the translocase, we followed the same procedure as described above but with ADP in the translocation mixture instead of ATP. This means that the only nucleotide these samples were exposed to after reconstitution was ADP and therefore no translocation would take place.

Sec translocases bound to pOmpA in the presence of ADP exhibited a broad height distribution with a peak at ~43 Å, which is in the range of SecA bound to SecYEG (Fig. 3A, black curve; image data shown in fig. S13). This represents an increase in peak height of about ~6 Å in comparison to translocase topography in the absence of precursors (Fig. 3A, green dashed curve). The number of intact translocases (i.e., SecYEG with SecA bound) remained similar to that found in the SecYEG-SecA starting material (72% versus 73%).

Sec translocases with pGBP and ADP exhibited a broad height distribution with a peak at ~53 Å, representing SecA bound to SecYEG (Fig. 3B, black curve). This peak height matches the peak height of the translocase with pGBP in the presence of ATP. As with ATP (Fig. 3B, red), there was an increase in peak height (~16 Å) in comparison to the starting material.

Overall, our results show that mean heights of active translocases engaging pOmpA moved to lower values in the hydrolysis and transition states (mean values plotted in Fig. 3C) compared to the reference state, reflecting the prevalence of SecA dissociation. In contrast, mean heights of active translocases engaging pGBP moved to higher values in all states (Fig. 3C). The large mean height change of active translocases engaging pGBP in both the resting (ADP) and hydrolysis state (ATP) from the reference state is suggestive of a prominent conformational change. However, volume analysis is required to distinguish a translocase conformational change from a change in the quaternary structure of SecA.

Oligomeric state of SecA in active translocase

We sought to quantify the quaternary structure of SecA in the active translocase. To do so, we restricted attention to membrane external protrusions that exhibited heights commensurate with translocase complexes, which range from ~32 to ~80 Å above the bilayer (Fig. 3, blue shaded regions) (13). To estimate the monomer volume of SecA,

we performed separate experiments with a mutant of SecA [SecAdN10, which has aminoacyl residues 2 to 11 deleted and which exists only as a monomer (40)] and quantitatively compared the results to simulations of AFM data. The volume peak for SecAdN10 on mica in the absence of any binding partners or a lipid bilayer was $0.35 \times 10^6 \text{ \AA}^3$ (fig. S9). This value may be considered to be a lower limit of the translocase volume because it does not account for binding SecYEG, SecB, ATP, or precursors. For comparison, a cross-linked SecA dimer (SecAC4Q801C) was also studied under similar conditions (fig. S9). Next, we produced simulated AFM images using SecA crystal structures and an approximate tip geometry (figs. S10 and S11). Figure S10 shows a peak agreement of approximately 90% between simulated images of monomeric SecA (Protein Data Bank code: 2FSF) and experimental SecAdN10 data, both of which were acquired in the absence of lipid (see Materials and Methods for details).

Further, we inspected the volumes of ~100 individual translocases that exhibited either single or double Gaussian-like profiles (fig. S8). The results indicated that SecA monomer volumes in the translocase were in the range between approximately 0.35×10^6 and $0.9 \times 10^6 \text{ \AA}^3$, whereas most dimers ranged between 0.9×10^6 and $2.0 \times 10^6 \text{ \AA}^3$. This monomeric volume range overlaps with measurements of the monomeric mutant SecAdN10 (fig. S9). Notwithstanding this agreement, interpretation of volumes is challenging because of factors including tip convolution and conformational dynamics such that AFM-measured volumes do not always reflect true volumes (34). With these caveats, we posit that the observed volume peak near $0.4 \times 10^6 \text{ \AA}^3$ (Fig. 2D) represents monomer SecA bound to SecYEG. Prominent shoulders around 1×10^6 to $2 \times 10^6 \text{ \AA}^3$ in the volume distributions for both pOmpA and pGBP (Fig. 2D) suggest the presence of SecA₂. Dimers (and higher-order oligomeric states) were also present in the translocase starting material, but to a lesser degree.

Having established approximate ranges for monomer and dimer volumes, we then analyzed translocases engaging either pOmpA or pGBP under different nucleotide conditions at the plateau stage of activity (Fig. 4). The volume distributions for ATP (red curve) or ADP (black curve) were broad with a peak around $\sim 1 \times 10^6$ to $1.5 \times 10^6 \text{ \AA}^3$ for both precursors. This volume range overlaps with that expected for a simulated SecA dimer (fig. S11), but was larger than what was measured for a cross-linked SecA dimer on mica alone (fig. S9), which may be due to the absence of lipid, ATP, precursor, and other binding partners, and/or the cross-linking itself. The translocase volume distributions also exhibited a substantial population of $>2 \times 10^6 \text{ \AA}^3$ (fig. S14 shows integrated distributions). This population could consist of extended conformations of dimers or quaternary structures larger than dimers, but aggregates may also be present. Hence, translocases exhibiting volumes $>2 \times 10^6 \text{ \AA}^3$ were excluded from further analysis. Irrespective of this broad range, volumes were similar for translocases engaging both precursors with either ATP or ADP bound. On the basis of these data, we conclude that SecA often exists as a dimer during the hydrolysis state (ATP) and resting state (ADP), independent of the two precursor species tested.

The same volume analysis applied to translocases exposed to ATP followed by ADPAIF shows notably different results (Fig. 4, A and B, blue dotted curves). These conditions produced a volume peak around $0.6 \times 10^6 \text{ \AA}^3$ for both precursors. This volume likely corresponds to a single SecA protomer bound to SecYEG (figs. S8 to S11). In the case of pOmpA, 42% of total protrusions were in the monomer volume range for samples with ATP followed by ADPAIF. In contrast, only 12% of protrusions in this dataset were in the monomer range for samples

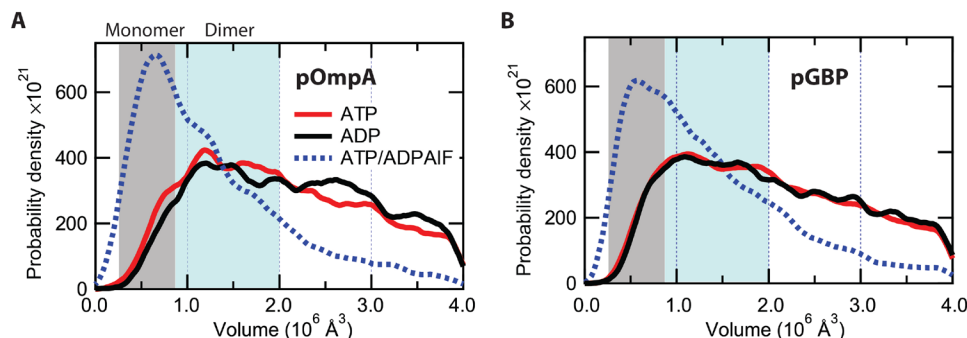


Fig. 4. Oligomeric state of SecA changes with nucleotide. (A) Volume distribution of translocase engaging pOmpA with different nucleotides: ADP only (black curve, $n = 1708$), ATP only (red curve, $n = 2518$), or ATP followed by ADPAIF (blue dotted curve, $n = 5088$). (B) Volume distribution of translocase engaging pGBP with different nucleotides: ADP only ($n = 2814$), ATP only ($n = 8441$), or ATP followed by ADPAIF ($n = 4973$). The approximate monomer and dimer volume ranges of SecA are indicated by the gray shaded region and blue shaded region, respectively.

with ATP or ADP alone. Similar behavior was observed for pGBP. In the case of pGBP, 39% were in the monomer volume range for samples with ATP followed by ADPAIF, and only 14% of total protrusions were in the monomer range for samples with ATP or ADP alone.

To summarize, for both precursors, we observed a >2-fold increase in SecA monomer population for samples probed at the transition state (ADPAIF) compared to the hydrolysis state (ATP) or resting state (ADP). These observations indicate that the oligomeric state of SecA in the translocase changes during the ATP hydrolysis cycle.

Topography of SecA₂ in the translocase varies with precursor species

Volume analysis indicated that dimeric SecA occupied the translocon during the hydrolysis and resting states for both pOmpA and pGBP, but what about the conformation of these translocases? To provide insight, we focused on heights of translocases in which SecA was in dimeric form, i.e., those exhibiting volumes within the range 0.9×10^6 to $2.0 \times 10^6 \text{ \AA}^3$ (Fig. 4, blue shaded regions). The resulting analyses with pGBP show that in the presence of either ADP or ATP, translocases exhibited single-peaked height distributions (Fig. 5, A and B). In contrast, translocases engaging pOmpA exhibited multimodal height distributions under the same conditions (Fig. 5, D and E). To quantify these distinctions, we used Bayesian information criterion to determine the optimal number of model distributions to fit each dataset (fig. S15). This analysis prescribed one gamma distribution for pGBP in either ATP or ADP. In contrast, three distributions were required for pOmpA subject to the same conditions. Gamma distributions were used because they naturally accommodate skewness inherent in the experimental data. In addition to the different number of modes, the peak locations for pGBP were shifted higher ($\sim 5 \text{ \AA}$) compared to pOmpA.

For both precursors, the primary differences between ATP and ADP appeared in an overall $\sim 3\text{-}\text{\AA}$ shift to higher heights in the presence of ATP, accompanied by an approximately 20% enhancement in the full width at half maximum of the height peaks. These changes, which were similar for both precursors, are likely attributable to conformational dynamics associated with ATP hydrolysis (33). We note the overall consistency for data collected with pOmpA in ATP and ADP, as well as with pGBP in ATP and ADP. These independent sets of experiments lead to the same conclusion—translocase conformation in the hydrolysis state and resting state varies for the precursor-bound species on the time scale of AFM imaging.

What is the origin of these different translocase conformations? Precursors can adopt structure and can also aggregate. Thus, conformational differences between the precursors themselves could be responsible. However, this is unlikely because the two precursors are similar in size (332 versus 346 aminoacyl residues for pGBP and pOmpA, respectively) and in design (disulfide-stabilized loop locations along the polypeptide chains are within two aminoacyl residues). Furthermore, translocase conformations in the presence of the transition state analog ADPAIF (Fig. 5, C and F) were distinct from those observed with either ADP or ATP for both precursors. In ADPAIF, which drives the system to monomer SecA, translocases engaged with pGBP exhibited a broader distribution, requiring two model distributions for optimal fitting. Under the same conditions, translocases engaged with pOmpA were also optimally fit by two distributions. Because the precursors do not exhibit ATPase activity, the nucleotide-dependent reversal in height distribution complexity—pGBP going from one distribution to two; pOmpA going from three to two—suggests that SecA is responsible for the underlying conformational distinctions.

A graphical summary of the results is presented (Fig. 6). SecA₂ in the translocase is the active species for both precursors. Once translocation has been stopped, one protomer (Fig. 6D) or both protomers of SecA (Fig. 6C) dissociate from translocase in the case of pOmpA. In contrast, only one protomer of SecA dissociates in the case of pGBP (Fig. 6E). In the cartoon, the dashed lines represent distinct conformational states that were stable over the time scale of AFM imaging ($\sim 500 \text{ ms}$ per molecule). Distinct states were apparent for pOmpA in ATP and ADP (Fig. 6, A and F) but were absent for pGBP, except in ADPAIF (Fig. 6E).

DISCUSSION

We imaged translocases at work under near-native conditions. AFM data complement high-resolution structures by providing a direct view of the Sec translocase engaging precursor proteins in a lipid bilayer and in aqueous buffer solution. Experiments showed translocase complexes undergoing significant topographic changes in a manner that depended on precursor species, nucleotide species, and stage of translocation.

AFM imaging requires the biological material to be adsorbed onto a surface such as mica. This can prompt questions about biological activity. Recently, we showed that the basal ATPase activity

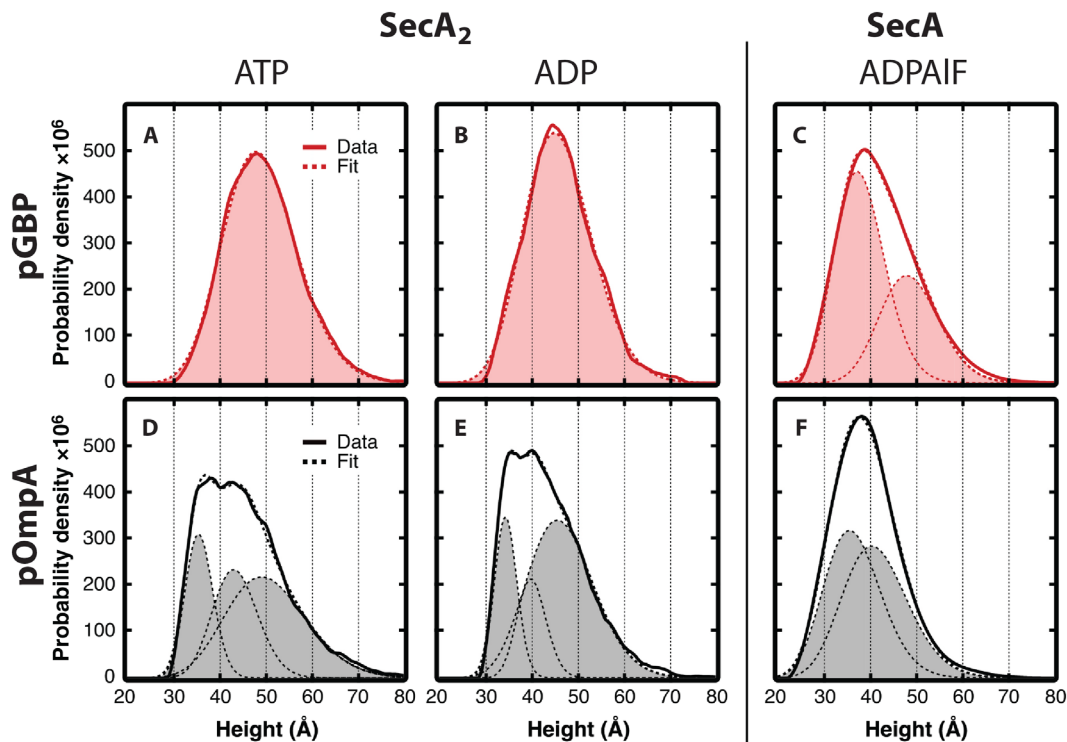


Fig. 5. Active translocase conformations differ with precursor species. Height distributions are shown for translocases engaging pGBP when exposed to (A) ATP ($n = 3431$), (B) ADP ($n = 1128$), or (C) ADPAIF ($n = 1860$), as well as translocases engaging pOmpA when exposed to (D) ATP ($n = 1047$), (E) ADP ($n = 661$), or (F) ADPAIF ($n = 2112$). Only translocases exhibiting volumes in the range corresponding to SecA₂ or SecA monomer were included, as indicated. Bayesian information criterion was used to determine the optimal number of gamma distributions for each fit. The analysis prescribed one gamma distribution for (A) and (B), two for (C) and (F), and three for (D) and (E).

of surface-adsorbed SecA is similar to solution activity (33). Here, we found that Sec translocases embedded in mica-supported lipid bilayers achieve ATP-driven translocation with a turnover number >1 . This is similar in magnitude to the turnover achieved in traditional translocation assays (14) and supports the notion that the visualization provided by AFM reflects active translocase conformations.

We carried out topographical investigations to follow the translocation reaction in a coarse-grained manner. At the initial stage of the reaction ($t = 30$ s), translocases engaging either pGBP or pOmpA exhibited similar distributions of height above the membrane (Fig. 2, B and F). Starting from this largely precursor-independent initial stage, many translocases engaging pOmpA displayed a substantial decrease in height at the plateau stage of translocation, revealing just SecYEG, indicative of complete SecA dissociation. For pGBP, most translocases remained intact and exhibited an increased height at plateau.

It has been previously reported that SecA binds tightly to the SecYEG/pOmpA complex but is readily released upon ATP hydrolysis (41). Our results are consistent with this notion. However, here, we show that the release of SecA is precursor dependent. Analysis revealed that in 44% of translocase complexes with pOmpA, SecA had completely dissociated from SecYEG; hence, only 56% of the total membrane-external cytoplasmic protrusions observed were active translocases (i.e., containing both SecYEG and SecA) when evaluated at the plateau stage of translocation. In contrast, for pGBP, 84% of complexes were active translocases at plateau. It would be informative to distinguish SecYEG containing jammed precursors (indicative of successful translocation to the precursor loop followed by translocase

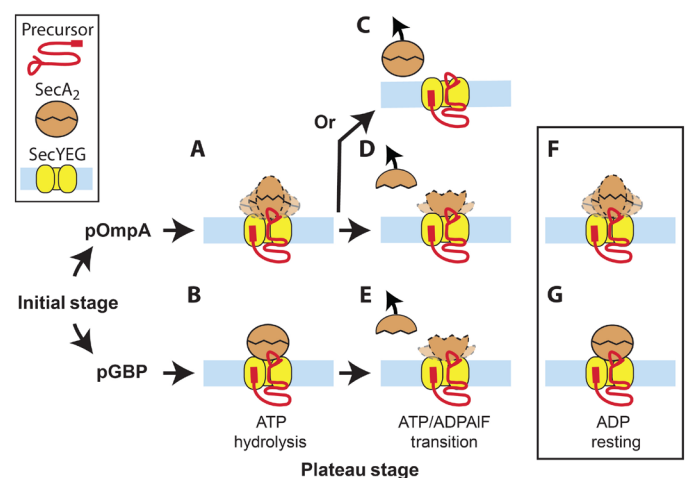


Fig. 6. Precursor-dependent model of translocase activity. We present a summary of results in cartoon form (not to scale) for pOmpA (A, C, D, F) or for pGBP (B, E, G) under the conditions listed. Individual components of the system include the following: precursor (red) with an N-terminal signal sequence and a disulfide-stabilized loop, SecA₂ (orange), and SecYEG (yellow) in a lipid bilayer (light blue). The dashed lines indicate distinct stable conformations on the time scale of AFM imaging. AFM measurements of the active Sec translocase do not provide direct visualization of SecYEG or the oligomeric state of SecYEG because it is buried underneath SecA. In the absence of this information, monomer SecYEG is drawn in all conditions. In addition, cartoons are not meant to accurately convey the orientation of SecA or SecA₂.

dissociation) from empty translocons. However, when imaged in fluid at room temperature, the conformational dynamics of the membrane-external cytoplasmic SecYEG loops (34) make distinguishing these two possibilities challenging.

The SecA that remained bound to the translocon during hydrolysis was observed to cycle between dimer and monomer in a manner that depended on nucleotide species but not on precursor species. In vitro and in vivo observations have shown that dimeric SecA is prevalent (19, 42), at least during the rate-limiting step of ATP hydrolysis, and that oligomeric state changes of SecA drive a critical step of the translocation process (2, 4). We showed that SecA₂ in the translocase dissociates to monomer in the presence of the transition state analog ADPAIF (Fig. 4) but remains dimeric (or higher order) in ATP or ADP. These results did not change substantially between the two precursor species that we studied. This is in agreement with previous work showing that precursor-stimulated ATP hydrolysis leads to SecA monomerization (2, 4). ATP hydrolysis is fast compared to ADP release (43); thus, many translocases imaged in the presence of ATP are expected to be similar to those in ADP. We note that the corresponding oligomeric states of SecYEG (or changes thereof) are largely concealed from the atomic force microscope tip by SecA in the AFM images.

The structure and dynamic conformations of SecA₂ in the active Sec translocase remain largely unknown and hinder understanding. Our single-molecule imaging data showed two model precursor proteins using different translocase conformations at a similar chemomechanical stage within the apparatus. The distribution of heights above the membrane surface for translocases in the hydrolysis state and resting state, both of which contain SecA₂, was trimodal when engaging pOmpA. The analogous height populations were taller and displayed a single prominent mode for translocases engaging pGBP. Conformational distinctions changed when the system was probed in the presence of a transition state analog. Because the precursors do not exhibit ATPase activity, the conformation differences are likely attributable to the ATPase SecA in the translocase.

What is the origin of the complex trimodal height distribution exhibited by translocases engaging pOmpA during hydrolysis? SecA₂ has been reported in at least three different orientations, and SecA protomers are thought to act independently (with little cooperativity) and to slide or to rotate about the interface through electrostatic and/or hydrophobic interactions (4, 7, 22–27). Hence, the complex height distribution could be related to different orientational states of the SecA dimer interface.

AFM measurements provide topographical corroboration for the significant precursor-dependent differences recently observed in the translocation reaction, including in the apparent rate constant and in the extent of precursor translocation (14). One interpretation of the AFM data is that pGBP and pOmpA are transported across the cytoplasmic membrane by mechanisms that are distinct. However, there remains the alternative possibility that all the mechanical steps required for translocation are the same for both precursors, but differing kinetics gives rise to our observations. For example, during hydrolysis, the system could spend substantially more time in one conformation when engaging pGBP compared to pOmpA. Further work with higher time resolution will be required to distinguish between these possibilities. In addition, it will be important to determine what physical property (or properties) of the precursor species is (are) responsible for the observed differences in the translocation process. Last, we point out that our AFM experiments on stalled

complexes at coarsely separated translocation stages were not designed to discriminate between translocation step models such as the “push and slide” mechanism and the Brownian ratchet. Future studies using continuous monitoring of individual translocases over time may provide insight into this question.

Overall, we report here the visualization of translocation machinery at work in near-native lipid bilayers. Our comparison of translocases engaging two different precursors side by side offers a direct view of this complex and dynamic process. Looking toward the future, high spatial-temporal precision single-molecule techniques are poised to shed further light on mechanisms underlying Sec system function.

MATERIALS AND METHODS

Purification of Sec components

SecYEG was purified from a strain C43 (DE3) suitable for overexpression of membrane protein (44) harboring a plasmid encoding SecE with a His-tag at the N terminus, SecYC329S, C385S, and SecG (45). Cells were broken by passage through a French pressure cell (5.5×10^7 Pa), and the membranes were isolated by centrifugation and solubilized in dodecyl- β -maltoside (DBM). SecYEG was purified by chromatography using a HisTrap column (GE Healthcare) and stored at -80°C in 20 mM Tris-Cl (pH 8), 0.3 M NaCl, 10% glycerol, 0.6% DBM, and 2 mM dithiothreitol (DTT). Wild-type SecA was purified as previously described (46) with the following modifications. Intact washed cells were incubated on ice for 30 min with 8 mM EDTA to chelate Mg^{2+} in the cell envelope. The cells were pelleted and washed twice to remove the EDTA before being lysed by three cycles of freezing and thawing in the presence of lysozyme. The removal of EDTA before lysis is crucial to prevent the extraction of zinc from SecA. Following centrifugation, SecA was purified from the relevant supernatants by chromatography. The cross-linked dimeric species SecAC4Q801C was purified as described above (this is SecA with the four natural cysteine residues changed to serine, C98S, C885S, C887S, C896S, and Q801C). SecAdN10 was purified as previously described (13). The purified proteins were dialyzed into 10 mM Hepes (pH 7.6), 0.3 M KAc, and 2 mM DTT and stored at -80°C . Cultures for SecB purification were grown as previously described (47), the cells were disrupted with a French press at 5.5×10^7 Pa, and the protein was purified from high-speed supernatants using a QAE column (TosoHaas). The purified SecB was stored in the same solution as used for SecA. Concentrations of the proteins were determined spectrophotometrically at 280 nm using coefficients of extinction as follows: SecB tetramer, $47,600 \text{ M}^{-1} \text{ cm}^{-1}$; SecA monomer, $78,900 \text{ M}^{-1} \text{ cm}^{-1}$; SecYEG, $45,590 \text{ M}^{-1} \text{ cm}^{-1}$.

Preparation of radiolabeled precursors

pOmpA and pGBP were produced in strain MM52 from plasmids (pAL612 and pAL663, respectively) carrying the *ompA* gene or the *mglB* gene altered to generate polypeptides with only two cysteine residues. In OmpA, C290 was substituted by serine and G244 was substituted by cysteine, and the native C302 was retained. For GBP, two cysteines were introduced, L267C and D310C. Proteins were radiolabeled by the addition of a mixture of ^{14}C -L-amino acids (PerkinElmer) to cells growing in M9 minimal media as previously described (14, 40). pOmpA was purified as previously described (14, 40). pGBP was purified as follows: Cells were disrupted with a French press, and inclusion bodies containing pGBP were collected by centrifugation, solubilized with urea,

and loaded onto a HiTrap QAE column (GE Healthcare). Precursors were stored at -80°C in 10 mM Hepes at pH 7.6 with 1 mM tris(2-carboxyethyl) phosphine (TCEP) to maintain the sulfhydryls in reduced form; for pOmpA, 0.1 M KAc and 4 M urea; and for pGBP, 0.3 M KAc, 1 N GnHCl, and 1 mM EGTA. After removal of TCEP, disulfide bond-stabilized loops were generated by the addition of 0.1 mM copper phenanthroline to the solution and incubation for 5 min on ice. Copper phenanthroline was removed using a NAP10 column (GE Healthcare).

Preparation of proteoliposomes

Lipids (*E. coli* polar lipid extract, Avanti) in chloroform were blown dry with N_2 and placed in a vacuum chamber overnight. A dry mechanical vacuum pump (XDS5, Edwards) was used to prevent back streaming of oil, a potential contaminant. Dried lipids were suspended in 10 mM Hepes (pH 7.6), 30 mM KAc, and 1 mM $\text{Mg}(\text{Ac})_2$. Unilamellar liposomes were prepared by extrusion through membranes (pore diameter, ~ 100 nm; LiposoFast, Avestin). To form proteoliposomes, the liposomes were swelled, but not disrupted, using a detergent-to-lipids ratio of 4.65 mM DBM/5 mM lipids (48). After swelling for 3 hours at room temperature, the proteins to be incorporated were added: SecYEG at 5 μM (the molar ratio of SecYEG to lipid was 1:1000), and for coassembly of SecA (SecYEG-SecA), SecA at 5 μM dimer. Incubation was continued for 1 hour at room temperature, followed by addition of Bio-Beads SM-2 (Bio-Rad) to remove the detergent. The proteoliposomes were isolated by centrifugation at 436,000g for 20 min at 4°C in a TL100.1 rotor (Beckman). The pellet was suspended in the same buffer and centrifuged again as earlier. The final pellet was suspended to give a concentration of ~ 10 mM lipid and 10 μM SecY. The suspension was stored at -80°C .

Translocation assay in solution

A time course of translocation assay was performed before each AFM experiment using the precursors containing disulfide-stabilized loops. Translocation of 1 μM oxidized pOmpA or pGBP, labeled with a ^{14}C -L-amino acid mixture, into proteoliposomes was carried out at 30°C under conditions of limiting SecY (1 μM) with SecA (1.2 μM dimer), SecB (1 μM tetramer), and EGTA (1 mM) to prevent pGBP from folding, as previously described (40), with the following modifications: An ATP-regenerating system consisting of 7.5 mM phosphocreatine and creatine phosphokinase (37 mg/ml) was present in the reaction. In addition, DTT was omitted from the reaction mix, and different nucleotides were added in the reaction mixture in place of ATP. In the case of ADP or ADPAIF, the ATP-regenerating system was omitted to prevent generation of ATP. A volume of sample selected for translocation quantification was subjected to proteinase K digestion. The radioactivity in the protein bands corresponding to protected precursors in the gels of the translocation assays was measured using a Fujifilm FLA 3000 PhosphorImager in the linear range of its response.

Translocation assay on mica

Proteoliposomes SecYEG-SecA (13) were exposed to 2 mM ATP for 15 min on ice. One hundred microliters of this solution was incubated on a freshly cleaved mica surface (V1 grade, Ted Pella Inc.) for 1 hour on ice (which matches the incubation used in AFM experiments). Surfaces were rinsed 10 times with 50 μl of buffer solution: 10 mM Hepes, 120 mM KAc, and 5 mM MgAc_2 (pH 7.6). Then, 50 μl of precursor mixture consisting of 1 μM radiolabeled pOmpA, 1 μM

SecB, 1 μM SecA, 3 mM ATP in 10 mM Hepes, 120 mM KAc, 5 mM MgAc_2 , 2 mM DTT, and 1 mM EGTA (pH 7.6) was added to the surface. Surfaces were then incubated at room temperature for 2 hours (which approximates the time scale of an AFM imaging session). This was followed by proteinase K incubation (70 μl at 19 U/ml for 15 min) and urea washing (150 ml at 6 M). Surfaces were then rinsed with 100 μl of buffer (10 times). Approximately 95% of the remaining solution was pipetted off the mica, which was then dried at 70°C for 20 min. We then exposed the mica to a phosphorus film (Fujifilm BAS-MS 2340) in a closed cassette for 48 hours followed by imaging (GE Healthcare Amersham Typhoon). Control experiments were performed in an identical manner to that described above, but in the absence of ATP in the precursor mixture. The amount of precursor was quantified using ImageQuant software. We created a standard curve of pixel intensity as a function of mol radioactive precursor by spotting known quantities of radioactive precursor on mica surfaces that were then dried and exposed to the phosphorus film under identical conditions as used to quantify translocation activity. The inverse slopes of the curves were computed and used to convert pixel intensity to pmol precursor.

Sample preparation for AFM imaging

Immediately before the addition of proteinase K in the translocation assay, aliquots of the reaction mixture were placed on ice and diluted with imaging buffer [10 mM Hepes (pH 7.6), 120 mM KAc, and 5 mM MgAc_2] to 0.1 μM SecY. Then, 100 μl of this diluted sample was deposited onto freshly cleaved mica (Ted Pella Inc.) and incubated for 1 hour on ice. During this time, proteoliposomes ruptured and formed two-dimensional supported lipid bilayers that are amenable to AFM imaging (34). Before AFM imaging, the sample was washed three times using 100 μl of imaging buffer to remove unadsorbed material.

AFM imaging

AFM images were acquired in imaging buffer in tapping mode using a commercial instrument (Cypher, Asylum Research). Biolever mini tips (BL-AC40TS, Olympus) with measured spring constants ~ 0.06 N/m were used. Images were recorded at $\sim 32^{\circ}\text{C}$ with an estimated tip-sample force of < 100 pN, deduced by comparing the free space tapping amplitude (~ 5 nm) to the imaging set point amplitude (~ 4 nm). AFM images were acquired with the following parameters: 512×512 pixels; scan size, 1 to $4 \mu\text{m}^2$; and scan speed, 10 to 11 nm/ms, except for Fig. 1E data with 256×256 pixels; scan size, $0.4 \mu\text{m}^2$; and scan speed, 83 nm/ms. We analyzed at least 10 images per condition studied (i.e., precursor species, nucleotide species, and translocation stage), at least three independent experiments/mica stages/sample preparations per condition, and at least two different tips for each condition. Note that tips were recovered after each experiment and cleaned for reuse.

AFM analysis

As is common in AFM analysis, images were flattened (first order) to minimize background tilt. To identify and precisely measure individual protrusions above the lipid bilayer, a custom algorithm was used (Igor Pro 6.3). AFM images were first partitioned into 500 nm by 500 nm segments, each of which was analyzed separately to produce more consistent background conditions. A height threshold was used to separate protrusions from the background lipid bilayer. The height threshold was determined dynamically for each segment

such that every pixel above the threshold was more than two SDs above the measured RMS noise level. A flood-fill algorithm was then used to identify sets of connected pixels above the height threshold, defining a protrusion and its boundary. Voids were discarded from analysis by virtue of their negative heights (as measured from the upper bilayer surface). Individual protrusions were then extracted from the full-scale image and further processed individually, first with a local first-order flattening to minimize local background tilt and then with a streak-removal algorithm. This algorithm corrected for the “parachuting” effect of the atomic force microscope tip in which the tip loses contact with the surface, generating horizontal “streak” artifacts. To identify and eliminate these artifacts, single-pixel high streaks (along a single scan line) were identified, removed, and replaced by averaging neighboring pixels. To calculate the volume of a single protrusion, a set height threshold of 500 pm above the calculated background level was used to separate protein protrusion pixels from background pixels. A fixed height threshold, as opposed to the dynamic height threshold used to originally detect the protrusion, was used to maintain consistency between volume measurements of all protrusions. The volume was then calculated by summing the height of all pixels in the protrusion and scaling by the pixel dimensions to effectively integrate under the protrusion. For height calculations, the height of a protrusion was calculated as the average height of the top 10% highest pixels in the protrusion minus the background level. The averaging was used to reduce the influence of single pixel noise on the height measurement. The entire process, including processing and segmenting of the raw image, protrusion detection, and height and volume measurements, was completed automatically. Bayesian information criterion was implemented in Igor Pro 7 to determine the optimal number of subpopulations for each dataset and avoid overfitting (49). Bootstrapping was used to estimate errors of reported population percentages. In all cases, these errors were <1%. Probability density plots were normalized to integrate to unity when units of the abscissa were expressed in meters or cubic meters (i.e., for height or volume distributions, respectively).

Simulations of AFM images

Simulated AFM images were produced by modeling the interaction between a biomolecule and the atomic force microscope tip during the imaging process. The action of “scanning” the atomic force microscope tip across a sample surface to produce an image is captured mathematically by the morphological dilation operation, which is responsible for the convolution effect seen in AFM imagery by tips that are not perfectly sharp. To construct a simulated AFM image of SecA, we explicitly computed the morphological dilation between three-dimensional models of SecA and an atomic force microscope tip. SecA was modeled via its x-ray crystal structure where each atom was modeled as a sphere with the van der Waals radius (50). The atomic force microscope tip was modeled as a cone with a rounded, spherical tip with a cone angle of 17.5° and a tip radius of 6 nm. A simulated AFM image was then produced using custom software (Igor Pro 7, WaveMetrics, Portland, OR). To compare simulated and experimental images, the residual between the images was squared and integrated, with the square root of the result then used to quantify the discrepancy between the images. The discrepancy was normalized as a percentage of the total volume of the experimental image. We then defined the percent agreement as one minus the normalized discrepancy. The agreement was maximized over all relative orientations (translations and rotations) between the exper-

imental and simulated images. **Code availability:** The code used in this study is available from the corresponding author upon request.

SUPPLEMENTARY MATERIALS

Supplementary material for this article is available at <http://advances.sciencemag.org/cgi/content/full/5/6/eaav9404/DC1>

Fig. S1. Traditional translocation assays.
 Fig. S2. Calibration of surface translocation assays.
 Fig. S3. Surface translocation assays.
 Fig. S4. AFM images of Sec translocases engaging precursors at the initial stage of activity.
 Fig. S5. AFM Images of Sec translocases engaging precursors at the plateau stage of activity.
 Fig. S6. Liposomes alone and liposomes containing just SecYEG.
 Fig. S7. Translocase topography at lower protein-to-lipid (P:L) ratio.
 Fig. S8. Representative Sec translocase monomers and dimers.
 Fig. S9. SecA monomers and dimers without SecYEG.
 Fig. S10. Simulated images of monomeric SecA and comparison to experiment.
 Fig. S11. Simulated AFM images of SecA monomers in different conformations and dimeric SecA.
 Fig. S12. Representative AFM images of Sec translocases with ATP.
 Fig. S13. Representative AFM images of Sec translocases with ADP.
 Fig. S14. Integrated volume histograms.
 Fig. S15. Model optimization using Bayesian information criterion.

REFERENCES AND NOTES

1. J. M. Crane, L. L. Randall, The sec system: Protein export in *Escherichia coli*. *EcoSal Plus* **7**, 10.1128/ecosalplus.ESP-0002-2017 (2017).
2. A. Tsigotaki, J. de Geyter, N. Soštaric, A. Economou, S. Karamanou, Protein export through the bacterial Sec pathway. *Nat. Rev. Microbiol.* **15**, 21–36 (2017).
3. K. Morita, H. Tokuda, K.-i. Nishiyama, Multiple SecA molecules drive protein translocation across a single translocon with SecG inversion. *J. Biol. Chem.* **287**, 455–464 (2012).
4. G. Gouridis, S. Karamanou, M. F. Sardis, M. A. Schärer, G. Capitani, A. Economou, Quaternary dynamics of the SecA motor drive translocase catalysis. *Mol. Cell* **52**, 655–666 (2013).
5. B. W. Bauer, T. Shemesh, Y. Chen, T. A. Rapoport, A “push and slide” mechanism allows sequence-insensitive translocation of secretory proteins by the SecA ATPase. *Cell* **157**, 1416–1429 (2014).
6. J. Young, F. Duong, Investigating the stability of the SecA–SecYEG complex during protein translocation across the bacterial membrane. *J. Biol. Chem.* **294**, 3577–3587 (2019).
7. J. F. Hunt, S. Weinkauff, L. Henry, J. J. Fak, P. McNicholas, D. B. Oliver, J. Deisenhofer, Nucleotide control of interdomain interactions in the conformational reaction cycle of SecA. *Science* **297**, 2018–2026 (2002).
8. A. R. Osborne, W. M. Clemons Jr., T. A. Rapoport, A large conformational change of the translocation ATPase SecA. *Proc. Natl. Acad. Sci. U.S.A.* **101**, 10937–10942 (2004).
9. J. Zimmer, Y. Nam, T. A. Rapoport, Structure of a complex of the ATPase SecA and the protein-translocation channel. *Nature* **455**, 936–943 (2008).
10. K. J. Erlandson, S. B. M. Miller, Y. Nam, A. R. Osborne, J. Zimmer, T. A. Rapoport, A role for the two-helix finger of the SecA ATPase in protein translocation. *Nature* **455**, 984–987 (2008).
11. W. J. Allen, R. A. Corey, P. Oatley, R. B. Sessions, S. A. Baldwin, S. E. Radford, R. Tuma, I. Collinson, Two-way communication between SecY and SecA suggests a Brownian ratchet mechanism for protein translocation. *eLife* **5**, e15598 (2016).
12. F.-C. Liang, U. K. Bageshwar, S. M. Musser, Bacterial Sec protein transport is rate-limited by precursor length: A single turnover study. *Mol. Biol. Cell* **20**, 4256–4266 (2009).
13. C. Mao, C. E. Cheadle, S. J. S. Hardy, A. A. Lilly, Y. Suo, R. R. Sanganna Gari, G. M. King, L. L. Randall, Stoichiometry of SecYEG in the active translocase of *Escherichia coli* varies with precursor species. *Proc. Natl. Acad. Sci. U.S.A.* **110**, 11815–11820 (2013).
14. P. Bariya, L. L. Randall, Co-assembly of SecYEG and SecA fully restores the properties of the native translocon. *J. Bacteriol.* **201**, e00493-18 (2018).
15. D. Oliver, Substrate proteins take shape at an improved bacterial translocon. *J. Bacteriol.* **201**, e00618-18 (2019).
16. M. Akita, A. Shinkai, S.-i. Matsuyama, S. Mizushima, SecA, an essential component of the secretory machinery of *Escherichia coli*, exists as homodimer. *Biochem. Biophys. Res. Commun.* **174**, 211–216 (1991).
17. R. L. Woodbury, S. J. Hardy, L. L. Randall, Complex behavior in solution of homodimeric SecA. *Protein Sci.* **11**, 875–882 (2002).
18. E. Or, A. Navon, T. Rapoport, Dissociation of the dimeric SecA ATPase during protein translocation across the bacterial membrane. *EMBO J.* **21**, 4470–4479 (2002).
19. I. Kusters, G. van den Bogaart, A. Kedrov, V. Krasnikov, F. Fulyani, B. Poolman, A. J. M. Driessen, Quaternary structure of SecA in solution and bound to SecYEG probed at the single molecule level. *Structure* **19**, 430–439 (2011).

20. J. Benach, Y.-T. Chou, J. J. Fak, A. Itkin, D. D. Nicolae, P. C. Smith, G. Wittrock, D. L. Floyd, C. M. Golsaz, L. M. Gierasch, J. F. Hunt, Phospholipid-induced monomerization and signal-peptide-induced oligomerization of SecA. *J. Biol. Chem.* **278**, 3628–3638 (2003).
21. Z. Bu, L. Wang, D. A. Kendall, Nucleotide binding induces changes in the oligomeric state and conformation of Sec A in a lipid environment: A small-angle neutron-scattering study. *J. Mol. Biol.* **332**, 23–30 (2003).
22. V. Sharma, A. Arockiasamy, D. R. Ronning, C. G. Savva, A. Holzenburg, M. Braunstein, W. R. Jacobs Jr., J. C. Sacchettini, Crystal structure of *Mycobacterium tuberculosis* SecA, a preprotein translocating ATPase. *Proc. Natl. Acad. Sci. U.S.A.* **100**, 2243–2248 (2003).
23. J. Zimmer, W. Li, T. A. Rapoport, A novel dimer interface and conformational changes revealed by an X-ray structure of *B. subtilis* SecA. *J. Mol. Biol.* **364**, 259–265 (2006).
24. D. G. Vassilyev, H. Mori, M. N. Vassilyeva, T. Tsukazaki, Y. Kimura, T. H. Tahirov, K. Ito, Crystal structure of the translocation ATPase SecA from *Thermus thermophilus* reveals a parallel, head-to-head dimer. *J. Mol. Biol.* **364**, 248–258 (2006).
25. Y. Papanikolaou, M. Papadovasilaki, R. B. G. Ravelli, A. A. McCarthy, S. Cusack, A. Economou, K. Petratos, Structure of dimeric SecA, the *Escherichia coli* preprotein translocase motor. *J. Mol. Biol.* **366**, 1545–1557 (2007).
26. R. Singh, C. Kraft, R. Jaiswal, K. Sejwal, V. B. Kasaragod, J. Kuper, J. Bürger, T. Mielke, J. Lührink, S. Bhushan, Cryo-electron microscopic structure of SecA protein bound to the 70S ribosome. *J. Biol. Chem.* **289**, 7190–7199 (2014).
27. A. K. Yazdi, G. C. Vezina, B. H. Shilton, An alternate mode of oligomerization for *E. coli* SecA. *Sci. Rep.* **7**, 11747 (2017).
28. R. Lill, W. Dowhan, W. Wickner, The ATPase activity of SecA is regulated by acidic phospholipids, SecY, and the leader and mature domains of precursor proteins. *Cell* **60**, 271–280 (1990).
29. J. P. Hendrick, W. Wickner, SecA protein needs both acidic phospholipids and SecY/E protein for functional high-affinity binding to the *Escherichia coli* plasma membrane. *J. Biol. Chem.* **266**, 24596–24600 (1991).
30. B. T. Findik, V. F. Smith, L. L. Randall, Penetration into membrane of amino-terminal region of SecA when associated with SecYEG in active complexes. *Protein Sci.* **27**, 681–691 (2018).
31. C. A. Bippes, D. J. Muller, High-resolution atomic force microscopy and spectroscopy of native membrane proteins. *Rep. Prog. Phys.* **74**, 086601 (2011).
32. Y. F. Dufrene, T. Ando, R. Garcia, D. Alsteens, D. Martinez-Martin, A. Engel, C. Gerber, D. J. Müller, Imaging modes of atomic force microscopy for application in molecular and cell biology. *Nat. Nanotechnol.* **12**, 295–307 (2017).
33. N. Chada, K. Chattrakun, B. P. Marsh, C. Mao, P. Bariya, G. M. King, Single molecule observation of nucleotide induced conformational changes in basal SecA-ATP hydrolysis. *Sci. Adv.* **4**, eaat8797 (2018).
34. R. R. Sanganna Gari, N. C. Frey, C. Mao, L. L. Randall, G. M. King, Dynamic structure of the translocon SecYEG in membrane: Direct single molecule observations. *J. Biol. Chem.* **288**, 16848–16854 (2013).
35. N. Chada, K. P. Sigdel, R. R. Sanganna Gari, T. R. Matin, L. L. Randall, G. M. King, Glass is a viable substrate for precision force microscopy of membrane proteins. *Sci. Rep.* **5**, 12550 (2015).
36. K. Uchida, H. Mori, S. Mizushima, Stepwise movement of preproteins in the process of translocation across the cytoplasmic membrane of *Escherichia coli*. *J. Biol. Chem.* **270**, 30862–30868 (1995).
37. B. W. Koenig, S. Krueger, W. J. Orts, C. F. Majkrzak, N. F. Berk, J. V. Silverton, K. Gawrisch, Neutron reflectivity and atomic force microscopy studies of a lipid bilayer in water adsorbed to the surface of a silicon single crystal. *Langmuir* **12**, 1343–1350 (1996).
38. K. J. Erlandson, E. Or, A. R. Osborne, T. A. Rapoport, Analysis of polypeptide movement in the SecY channel during SecA-mediated protein translocation. *J. Biol. Chem.* **283**, 15709–15715 (2008).
39. D. J. Müller, A. Engel, The height of biomolecules measured with the atomic force microscope depends on electrostatic interactions. *Biophys. J.* **73**, 1633–1644 (1997).
40. C. Mao, S. J. S. Hardy, L. L. Randall, Maximal efficiency of coupling between ATP hydrolysis and translocation of polypeptides mediated by SecB requires two protomers of SecA. *J. Bacteriol.* **191**, 978–984 (2009).
41. J. de Keyzer, C. van der Does, T. G. Kloosterman, A. J. M. Driessen, Direct demonstration of ATP-dependent release of SecA from a translocating preprotein by surface plasmon resonance. *J. Biol. Chem.* **278**, 29581–29586 (2003).
42. T. Banerjee, C. Lindenthal, D. Oliver, SecA functions in vivo as a discrete anti-parallel dimer to promote protein transport. *Mol. Microbiol.* **103**, 439–451 (2017).
43. J. J. Fak, A. Itkin, D. D. Ciobanu, E. C. Lin, X.-J. Song, Y.-T. Chou, L. M. Gierasch, J. F. Hunt, Nucleotide exchange from the high-affinity ATP-binding site in SecA is the rate-limiting step in the ATPase cycle of the soluble enzyme and occurs through a specialized conformational state. *Biochemistry* **43**, 7307–7327 (2004).
44. B. Miroux, J. E. Walker, Over-production of proteins in *Escherichia coli*: Mutant hosts that allow synthesis of some membrane proteins and globular proteins at high levels. *J. Mol. Biol.* **260**, 289–298 (1996).
45. K. S. Cannon, E. Or, W. M. Clemons Jr., Y. Shibata, T. A. Rapoport, Disulfide bridge formation between SecY and a translocating polypeptide localizes the translocation pore to the center of SecY. *J. Cell Biol.* **169**, 219–225 (2005).
46. L. L. Randall, J. M. Crane, A. A. Lilly, G. Liu, C. Mao, C. N. Patel, S. J. S. Hardy, Asymmetric binding between SecA and SecB two symmetric proteins: Implications for function in export. *J. Mol. Biol.* **348**, 479–489 (2005).
47. L. L. Randall, T. B. Topping, V. F. Smith, D. L. Diamond, S. J. S. Hardy, [35] SeeB: A chaperone from *Escherichia coli*. *Meth. Enzymol.* **290**, 444–459 (1998).
48. O. Lambert, D. Levy, J.-L. Ranck, G. Leblanc, J.-L. Rigaud, A new “gel-like” phase in dodecyl maltoside-lipid mixtures: Implications in solubilization and reconstitution studies. *Biophys. J.* **74**, 918–930 (1998).
49. G. Schwarz, Estimating the dimension of a model. *Ann. Stat.* **6**, 461–464 (1978).
50. S. Alvarez, A cartography of the van der Waals territories. *Dalton Trans.* **42**, 8617–8636 (2013).

Acknowledgments: We are grateful to all members of the Randall and King laboratories for discussions. **Funding:** This work was supported by an endowment from the Hugo Wurdack Trust at MU and the National Institutes of Health grant GM29798 (to L.L.R.) and by the National Science Foundation CAREER Award 1054832 (to G.M.K.) and a Burroughs Wellcome Fund Career Award at the Scientific Interface (to G.M.K.). **Author contributions:** R.R.S.G. performed the AFM experiments. K.C. and C.M. performed biochemical assays and analysis. B.P.M. developed software and applied analysis tools. N.C. performed experiments. R.R.S.G., K.C., C.M., B.P.M., N.C., L.L.R., and G.M.K. analyzed data and wrote the paper. G.M.K. supervised the project. All authors reviewed the paper. **Competing interests:** The authors declare that they have no competing interests. **Data and materials availability:** All data needed to evaluate the conclusions in the paper are present in the paper and/or the Supplementary Materials. Additional data related to this paper may be requested from the authors.

Submitted 2 November 2018

Accepted 9 May 2019

Published 12 June 2019

10.1126/sciadv.aav9404

Citation: R. R. Sanganna Gari, K. Chattrakun, B. P. Marsh, C. Mao, N. Chada, L. L. Randall, G. M. King, Direct visualization of the *E. coli* Sec translocase engaging precursor proteins in lipid bilayers. *Sci. Adv.* **5**, eaav9404 (2019).

Direct visualization of the *E. coli* Sec translocase engaging precursor proteins in lipid bilayers

Raghavendar Reddy Sanganna Gari, Kanokporn Chattrakun, Brendan P. Marsh, Chunfeng Mao, Nagaraju Chada, Linda L. Randall and Gavin M. King

Sci Adv 5 (6), eaav9404.
DOI: 10.1126/sciadv.aav9404

ARTICLE TOOLS	http://advances.sciencemag.org/content/5/6/eaav9404
SUPPLEMENTARY MATERIALS	http://advances.sciencemag.org/content/suppl/2019/06/10/5.6.eaav9404.DC1
REFERENCES	This article cites 49 articles, 18 of which you can access for free http://advances.sciencemag.org/content/5/6/eaav9404#BIBL
PERMISSIONS	http://www.sciencemag.org/help/reprints-and-permissions

Use of this article is subject to the [Terms of Service](#)

Science Advances (ISSN 2375-2548) is published by the American Association for the Advancement of Science, 1200 New York Avenue NW, Washington, DC 20005. The title *Science Advances* is a registered trademark of AAAS.

Copyright © 2019 The Authors, some rights reserved; exclusive licensee American Association for the Advancement of Science. No claim to original U.S. Government Works. Distributed under a Creative Commons Attribution NonCommercial License 4.0 (CC BY-NC).